

A Semi-Supervised CNN Method for SAR Image Recognition

Zhenyu Yue¹, Fei Gao^{1*}, Qingxu Xiong¹, Jun Wang¹, Teng Huang¹, Erfu Yang², Huiyu Zhou³

Abstract

Background / introduction: SAR image automatic target recognition technology (SAR-ATR) is one of the research hotspots in the field of image cognitive learning. Inspired by the human cognitive process, experts have designed convolutional neural networks (CNN) based methods and successfully applied the methods to SAR-ATR. However, the performance of CNNs significantly deteriorates when the labelled samples are insufficient.

Methods: To effectively utilize the unlabelled samples, a semi-supervised CNN method is proposed in this paper. First, CNN is used to extract the features of the samples, and subsequently the class probabilities of the unlabelled samples are computed using the softmax function. To improve the effectiveness of the unlabelled samples, we remove possible noise performing thresholding on the class probabilities. Afterwards, based on the remaining class probabilities, the information contained in the unlabelled samples is integrated with the scatter matrices of the standard linear discriminant analysis (LDA) method. The loss function of CNN consists of a supervised component and an unsupervised component, where the supervised component is created using the cross-entropy function and the unsupervised component is created using the scatter matrices. The class probabilities are utilized to control the impact of the unlabelled samples in the training process, and the reliability of the unlabelled samples is further improved.

Results: We choose ten types of targets from the Moving and Stationary Target Acquisition and Recognition (MSTAR) dataset. The experimental results show that the recognition accuracy of

*Corresponding Author, E-mail: feigao2000@163.com, Tel: +86-010-82317240, Fax: +86-010-82317240

¹ School of Electronic Information Engineering, Beihang University, Beijing 100191, China

² Strathclyde Space Institute, Department of Design, Manufacture and Engineering Management, University of Strathclyde, Glasgow G1 1XJ, UK

³ Department of Informatics, University of Leicester, Leicester, LE1 7RH, UK

our method is significantly higher than that of the supervised CNN method.

Conclusions: It proves that our method can effectively improve the SAR-ATR accuracy despite the deficiency of the labelled samples.

Key words: SAR image recognition, convolutional neural network, semi-supervised learning, linear discriminant analysis

1. Introduction

Synthetic Aperture Radar (SAR) has been widely used due to its high resolution and penetrating ability [1-3]. SAR image automatic target recognition technology (SAR-ATR) is one of the research hotspots in the field of image cognitive learning [4,5]. Based on the cognitive system, humans are able to recognize targets quickly and accurately. Inspired by this, various methods that imitate the human cognitive system have been proposed to improve the SAR-ATR accuracy.

The image cognitive system of humans is based on neural networks [6]. Image signals acquired by the retina first go through the primary visual cortex for extracting edge and orientation features, followed by the generation of shape and contour features. In this way, image signals pass through the higher level visual cortex and we can obtain the more abstract features. Hence, human image cognition is a process of obtaining abstract features through layer-by-layer visual cortex [7,8]. Inspired by this process, people have established various neural network models. By simulating the whole process of the human vision system from the retina to the visual cortex, an effective SAR image feature extraction method was proposed in [9]. Using the hierarchical perceptual inference process embedded in the cortex, Spratling et al proposed a hierarchical neural network for visual object recognition [10]. Ren et al. proposed a multiple convolutional neural

network (CNN) based on the human visual system (HVS) [11]. CNN simulates the visual cortex using convolution layers and each convolution layer contains several convolution kernels for extracting abstract features of the image data. Compared with the other neural network models, CNN has been successfully applied to SAR-ATR due to its powerful feature extraction capability [12-14].

Chen et al. designed a CNN model with a single layer to automatically extract features for SAR target recognition [15]. SAR images are transformed into a set of feature maps after certain convolution and pooling operation. Subsequently, the feature maps are used to train the softmax classifier. Gao et al. proposed a new SAR-ATR method by combining CNN and Support Vector Machine (SVM) [16]. The experimental results prove that the proposed method can achieve an average accuracy of 99% on ten types of targets. However, the CNN model needs a large number of labelled samples in the training process. When the labelled samples are insufficient, the recognition accuracy of the CNN decreases significantly [17]. Because of the imaging nature, speckle noise and clutters exist in SAR images and the outline of the targets is weak, which increases the difficulty of the sample annotation. As a result, the number of the labelled samples is insufficient, which restricts the application of CNN in SAR-ATR. In recent years, researches have focused on improving the SAR-ATR's accuracy with a small labelled dataset. In [18], the center loss is adopted and combined with the softmax loss to train the deep CNN. However, compared with labelled samples, unlabelled samples are easy to acquire. Besides, unlabelled samples also contain a wealth of information which helps to improve the SAR-ATR's accuracy.

Human cognition does not need a large number of labelled samples, Inspired by this mechanism, people have designed semi-supervised learning methods to improve the SAR-ATR

accuracy when the labelled samples are insufficient [22,23]. The commonly used semi-supervised learning methods include self-training, co-training, graph-based methods, and semi-supervised support vector machines [24-26]. Lv et al. proposed a semi-supervised predictive sparse decomposition method for feature learning [27]. To solve the online semi-supervised learning problems, Ding et al. proposed a novel manifold regularized model in a reproducing kernel Hilbert space [28].

Recently, researchers are focusing on combining semi-supervised learning methods with neural network models. To effectively utilize the unlabelled samples, a semi-supervised deep learning model based on ladder networks was proposed in [29]. Consisting of a corrupted encoder, a clean encoder and a decoder, the proposed model is trained to minimize the sum of the supervised loss function and the unsupervised loss function. Samuli and Timo proposed two simple and efficient semi-supervised CNN models, i.e. the Pi and the temporal ensembling models [30]. The two models are based on the self-ensembling method, where the predicted labels of the unlabelled samples are generated using the output of CNN at different epochs. According to the predicted labels, the unlabelled components of the loss function are obtained. The experimental results show that the two models improve the image recognition accuracy greatly when the labelled samples are insufficient. Although the above semi-supervised methods are proved to be effective, it is found that semi-supervised methods cannot always improve the image recognition accuracy because of the noise and interference in the unlabelled samples [31,32]. For example, the Pi and the temporal ensembling models use CNN to predict the labels of the unlabelled samples. However, the reliability of the unlabelled samples is significantly reduced if the predicted labels are incorrect. As a result, the recognition accuracy of CNN will be worse. The reliability of the

unlabelled samples restricts the application of semi-supervised methods in image recognition.

In this paper, a new semi-supervised CNN method is proposed to improve the SAR-ATR accuracy when the labelled samples are insufficient. First, CNN is used to extract the features of the samples, and the class probabilities of the unlabelled samples are obtained using the softmax function. In order to improve the reliability of the unlabelled samples, we perform thresholding processing on the class probabilities. Afterwards, based on the class probabilities, the information contained in the unlabelled samples is integrated with the scatter matrices of the standard LDA method. The loss function of CNN consists of a supervised and an unsupervised component. The supervised component is created by the cross-entropy function and the unsupervised component is created using the scatter matrices. The class probabilities are utilized to control the impact of the unlabelled samples in the training process, and the reliability of the unlabelled samples can be further improved.

The rest of this paper is arranged as follows. In section 2, CNN and the LDA methods are briefly introduced. Section 3 describes the principle of our proposed method in detail. The experiments based on the MSTAR database are performed in Section 4. Finally, we summarize our contribution in section 5.

2. Preliminary

2.1 Convolutional Neural Network

CNN is mainly composed of convolution, pooling and fully connected layers. The convolution layers are used to extract image features. The pooling layers decrease the risk of overfitting by reducing the number of features, and the fully connected layers are used to integrate the image features. The training process of CNN consists of forward and backward propagation

[33,34].

In the forward propagation process, the current layer of CNN receives the output of the previous layer, which is expressed as follows:

$$\left. \begin{aligned} z^l &= w^l a^{l-1} + b^l \\ a^l &= \sigma(z^l) \end{aligned} \right\} \quad (1)$$

where l denotes the l^{th} layer. z^l , w^l and b^l represent the weighted input of the l^{th} layer, the weight matrix and the bias matrix, respectively. σ denotes the nonlinear activation function and a^l represents the actual output value of the l^{th} layer. If $l=1$, a^0 represents the pixel value of the input image.

In the backpropagation process, the parameters w^l and b^l of CNN are updated using the back propagation (BP) algorithm. In detail, the BP algorithm firstly constructs a loss function based on the actual and the expected output of CNN. Afterwards, the gradient descent method is utilized to update the parameters w^l and b^l along the gradient decent direction of the loss function. Suppose that E_0 is the loss function and L denotes the number of the layers of CNN, the error vector of the output layer is expressed as follows:

$$\delta^L = \frac{\partial E_0}{\partial z^L} \quad (2)$$

The error vector of the $(l-1)^{\text{th}}$ layer can be calculated from the error vector of the l^{th} layer.

Therefore, the error vector δ^l of each layer can be calculated by the Chain Rule:

$$\delta^l = w^{l+1} \delta^{l+1} \circ \sigma'(z^l) \quad (3)$$

where the symbolic \circ represents the element-wise product of the two vectors. The partial derivative of E_0 to w^l and b^l can be calculated by Eqs. (1) and (3):

$$\left. \begin{aligned} \frac{\partial E_0}{\partial w^l} &= \frac{\partial E_0}{\partial z^l} \circ \frac{\partial z^l}{\partial w^l} = \delta^l \circ a^{l-1} \\ \frac{\partial E_0}{\partial b^l} &= \frac{\partial E_0}{\partial z^l} \circ \frac{\partial z^l}{\partial b^l} = \delta^l \end{aligned} \right\} \quad (4)$$

Then, the change values of w^l and b^l are calculated:

$$\left. \begin{aligned} \Delta w^l &= -\eta \frac{\partial E_0}{\partial w^l} \\ \Delta b^l &= -\eta \frac{\partial E_0}{\partial b^l} \end{aligned} \right\} \quad (5)$$

Where η denotes the learning rate.

2.2 Linear Discriminant Analysis (LDA)

LDA is used to search a subspace where the samples of different classes are distant from each other while the samples of the same class are close to each other [35,36]. In case of binary classification, given the training dataset $D = \{(x_i, y_i)\}_{i=1}^m$, where x_i denotes the training samples and $y_i \in \{0,1\}$ denotes the label of the samples, m represents the number of the samples in the training dataset. Suppose that μ_i and C_i represent the mean vector and covariance matrices of the i^{th} class respectively, and w denotes the projection vector. In order to make the samples of the same class as close as possible in the subspace, $w^T C_0 w + w^T C_1 w$ should be small. While $\|w^T \mu_0 - w^T \mu_1\|_2^2$ should be large to make the samples of different classes as distant as possible.

Thus, taking these into consideration, we get the optimization objective function as follows.

$$J = \frac{\|w^T \mu_0 - w^T \mu_1\|_2^2}{w^T C_0 w + w^T C_1 w} = \frac{w^T (\mu_0 - \mu_1)(\mu_0 - \mu_1)^T w}{w^T (C_0 + C_1) w} \quad (6)$$

Then we define the within-class scatter matrix $S_w = C_0 + C_1$ and the between-class scatter matrix

$S_b = (\mu_0 - \mu_1)(\mu_0 - \mu_1)^T$. Then the objective function Eq. (6) can be rewritten as Eq. (7), which is

called the ‘‘generalized Rayleigh quotient’’ of S_w and S_b .

$$J = \frac{w^T S_b w}{w^T S_w w} \quad (7)$$

Next, the LDA algorithm is extended to the field of multi-classification. Suppose that there are N classes and the number of the samples of the i^{th} class is m_i . First, the total-class scatter matrix is defined as follows,

$$S_t = S_b + S_w = \sum_{i=1}^m (x_i - \mu)(x_i - \mu)^T \quad (8)$$

where m denotes the total number of the samples and μ represents the mean vector of all the samples. The within-class scatter matrix is defined as the sum of the covariance matrices for each class:

$$S_w = \sum_{i=1}^N C_i \quad (9)$$

According to Eqs. (8) and (9), the between-class scatter matrix is obtained:

$$S_b = S_t - S_w = \sum_{i=1}^N m_i (\mu_i - \mu)(\mu_i - \mu)^T \quad (10)$$

There are various ways to construct the optimization objective function of LDA for multi-classification, and one of the common ways is expressed in Eq. (7).

3. The proposed method

First, we define the system parameters. The training dataset consists of two parts: $X = [L, U] \in R^{d \times N}$, where $L = [x_1, x_2, \dots, x_l] \in R^{d \times l}$ represents the labelled dataset and $U = [x_{l+1}, x_{l+2}, \dots, x_{l+u}] \in R^{d \times u}$ represents the unlabelled dataset. d denotes the dimension of the samples. $N = l + u$ is the number of the training samples.

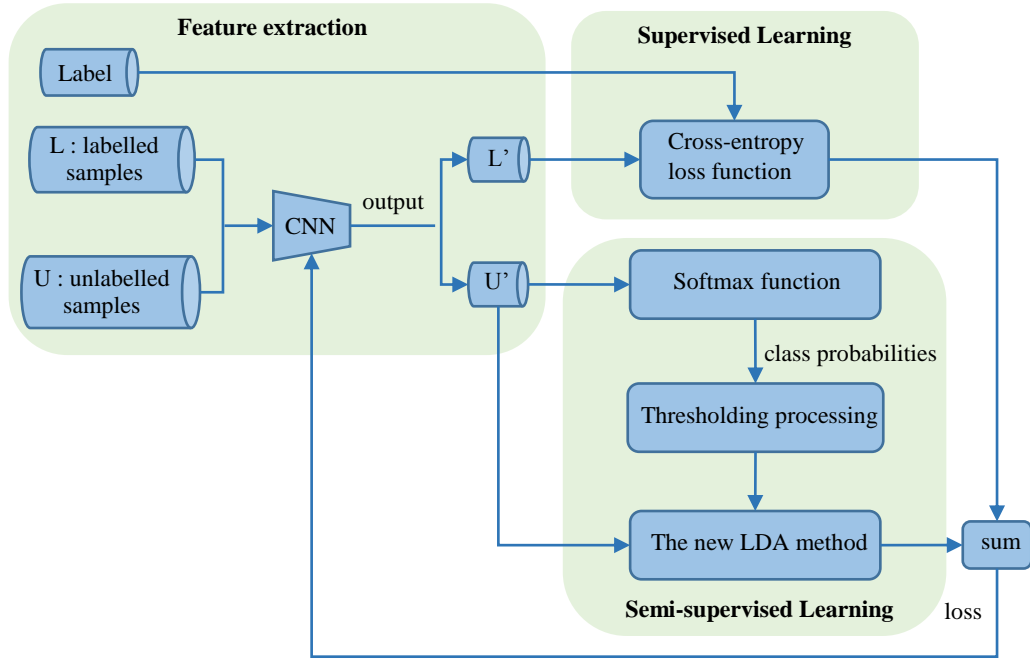


Figure 1: The flowchart of the training process

As shown in Figure 1, the training process of our method is composed of three parts: feature extraction, supervised learning and semi-supervised learning. In the feature extraction, we use CNN to extract the features of the samples. L' and U' represent the feature vector of the labelled and unlabelled datasets respectively. In the process of supervised learning, the labelled samples are utilized to obtain the supervised component of the loss function for CNN. The semi-supervised learning process which consists of two steps is the core of our method. First, we calculate the class probabilities of the unlabelled samples using the softmax function. To improve the reliability of the unlabelled samples, we perform thresholding processing on the class probabilities. Afterwards, based on the class probabilities, the information contained in the unlabelled samples is integrated to the scatter matrices of the standard LDA method, and the unsupervised component of the loss function is constructed using the scatter matrices. Next, the two steps of the semi-supervised learning process are analyzed in detail.

3.1 Class probabilities of unlabelled samples

To effectively utilize the unlabelled samples, we calculate the class probabilities at first. Since the samples in L and U are high-dimensional, we use CNN to extract the features so as to obtain the class probabilities. Compared with optical images, the signal to noise ratio (SNR) and resolutions of SAR images are relatively low. Therefore, CNN models such as AlexNet and VGGNet for optical images are not suitable for SAR images. As shown in Figure 2, we designed the CNN model for SAR images based on comprehensive experiments. The size of the input images is 64×64 . Conv1, Conv2 and Conv3 represent the convolution layers. The number of the convolution kernels in Conv1 is 20, and the kernel size is 3×3 . The number of the convolution kernels in Conv2 is 40, and the kernel size is 4×4 . The number of the convolution kernels in Conv3 is 80, and the kernel size is 3×3 . We adopt the Relu activation function in the convolution layers. Maxpool denotes the maximum pooling operation, and the pool size is 2×2 . The Flatten layer stretches the output of Conv3 to create a 2880 dimensional column vector. Linear1, Linear2 and Linear3 represent the fully connected layers. The output dimensions of each layer are 2880, 2880 and 10 respectively. The Relu activation function is also adopted in the fully connected layers.

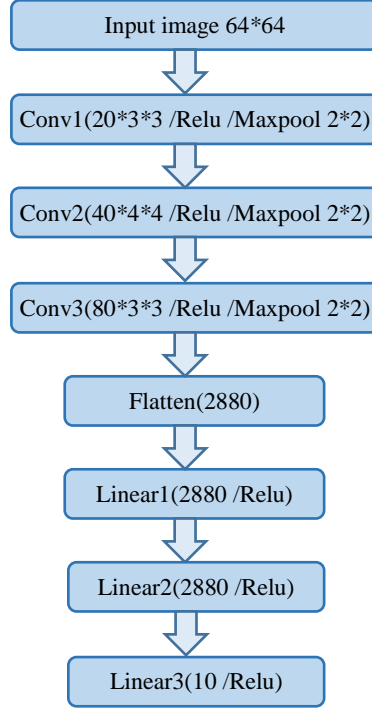


Figure 2: The CNN model employed in the proposed method.

Suppose that the number of the neurons in the output layer is K , that is, the CNN eventually divides the input images into K classes. As expressed in Eq. (11), we utilize the softmax function to normalize the output of CNN, and the class probabilities of the unlabelled samples are obtained.

$$p_k = \frac{e^{a_k}}{\sum_{j=1}^K e^{a_j}} \quad (11)$$

Where $[a_1, a_2, \dots, a_K]$ is the output of CNN. Hence, the class probabilities of a sample can be represented as $[p_1, p_2, \dots, p_K]$, where p_k denotes the probability of the sample belonging to the k^{th} class. The larger the value of p_k , the greater the probability that the sample belongs to the k^{th} class. $\sum_{k=1}^K p_k = 1$, and if one item increases, the sum of the others will be decreased.

The reliability of a sample is related to the probability that belongs to the class corresponding to its true label. We define the reliability factor (RF) to measure the reliability of samples. As expressed in equation Eq. (12), p_{true} denotes the probability of a sample belonging to the class

that corresponding to its true label. The larger the value of RF, the more reliable of a sample. In general, a sample with the RF value greater than 0.9 can be regarded as a reliable sample.

$$RF = \frac{P_{true}}{\sum_{k=1}^K P_k} \quad (12)$$

Suppose that $p^i \in R^{1 \times N}$ denotes the class probabilities of all the unlabelled samples belonging to the i^{th} class. To improve the reliability of the unlabelled samples, we apply thresholding processing to p^i :

$$p_j^i = \begin{cases} 0, & p_j^i < t \\ p_j^i, & \text{others} \end{cases}, i \in [1, 2, L, K], j \in [1, 2, L, u] \quad (13)$$

where p_j^i represents the j^{th} element of p^i and t is the threshold. The greater the value of t , the higher the reliability requirement for the unlabelled samples. If the maximum class probability of a sample is less than t , all the class probabilities of the sample will be set to 0. We utilize the unlabelled samples based on the class probabilities and the new LDA method. Thus, the unlabelled samples whose class probabilities are all set to 0 will not be utilized in the training process.

3.2 The new LDA method

After obtaining the class probabilities, how to effectively utilize the unlabelled samples is the key to improving the recognition accuracy of the CNN model. Most of the semi-supervised CNN methods extend the labelled dataset by using CNN to label the unlabelled samples. And the CNN is retrained using the extended dataset subsequently. However, when the initial labelled samples are insufficient, the generalization ability of the CNN model is weak. As a result, the ‘‘pseudo labels’’ for the unlabelled samples are not credible, which restricts the improvement of the recognition accuracy. In contrast, the LDA method constructs an optimization function based on

the within-class and between-class distance of the samples. Using the projection vector, the samples of different classes are distant from each other while the samples of the same class are close to each other. Here, we design a new LDA method to exploit the unlabelled samples. In our method, the information contained in the unlabelled samples is integrated to the scatter matrices of the standard LDA method based on the class probabilities. Then the unsupervised component of the loss function is calculated using the scatter matrices.

In the standard LDA method, if we map the samples to a space and assume that the density of each sample is 1. Then the mean vectors is used to denote the center of each class. We redefine the within-class mean vector u_i and the total mean vector u in the new LDA method:

$$\left. \begin{aligned} u_i &= \frac{\sum_{j=1}^N p_j^i x_j}{\sum_{j=1}^N p_j^i} = X \left(p_j^i / \sum_{j=1}^N p_j^i \right) = X \frac{\bar{p}^i}{\bar{p}} \\ u &= \frac{\sum_{i=1}^K \sum_{j=1}^N p_j^i x_j}{\sum_{i=1}^K \sum_{j=1}^N p_j^i} = X \left(\sum_{i=1}^K p^i / \sum_{i=1}^K \sum_{j=1}^N p_j^i \right) = X \frac{\bar{\circ} p}{\bar{p}} \end{aligned} \right\} \quad (14)$$

Compared with the standard LDA method, we use the class probabilities as the density of the unlabelled samples. The larger the probability of a sample belonging to a class, the greater the impact on the class center. Since the information contained in the unlabelled samples is effectively utilized, the mean vectors are more reliable.

Afterwards, we define the new scatter matrices:

$$\begin{aligned} S_b &= \sum_{i=1}^K m_i (u_i - u)(u_i - u)^T \\ &= X \left[\sum_{i=1}^K m_i \left(\frac{\bar{p}^i}{\bar{p}} - \bar{\circ} p \right) \left(\frac{\bar{p}^i}{\bar{p}} - \bar{\circ} p \right)^T \right] X^T \\ &= X \dot{S}_b X^T \end{aligned} \quad (15)$$

where $m_i = \sum_{j=1}^N p_j^i$,

$$\begin{aligned}
S_w &= \sum_{i=1}^k \sum_{j=1}^N p_j^i (x_j - u_i)(x_j - u_i)^T \\
&= X \left[\sum_{i=1}^k \sum_{j=1}^N p_j^i (h_j^i - \frac{1}{N} \mathbf{1})(h_j^i - \frac{1}{N} \mathbf{1})^T \right] X^T \\
&= X \dot{S}_w X^T
\end{aligned} \tag{16}$$

$$\begin{aligned}
S_t &= \sum_{i=1}^k \sum_{j=1}^N p_j^i (x_j - u)(x_j - u)^T \\
&= X \left[\sum_{i=1}^k \sum_{j=1}^N p_j^i (h_j^i - \hat{p})(h_j^i - \hat{p})^T \right] X^T \\
&= X \dot{S}_t X^T
\end{aligned} \tag{17}$$

where h_j^i is expressed as follows:

$$h_j^i = \begin{cases} 1, & i = j \\ 0, & \text{else} \end{cases} \tag{18}$$

Compared with the scatter matrices of the standard LDA method, we redefined the m_i in the between-class scatter matrix. In addition, the class probability p_j^i is added as the weight coefficient in the within-class and total-class scatter matrices. The greater the class probabilities of the unlabelled samples, the greater the impact on the scatter matrices. The new LDA method controls the impact of the unlabelled samples through the class probabilities. Thus, the reliability of the unlabelled samples is improved.

When constructing the ‘‘generalized Rayleigh quotient’’ optimization function, we can use any two scatter matrices, and one of the common ways is expressed in Eq. (19).

$$J = \frac{W^T S_w W}{W^T S_b W} \tag{19}$$

where $W = (w_1, w_2, \dots, w_K)$ denotes the projection matrix. Since both the numerator and denominator of Eq. (19) are matrices, the optimization function cannot be optimized as a scalar function. Therefore, an alternative optimization function is adopted:

$$J^* = \prod_{i=1}^K \frac{w_i^T S_b w_i}{w_i^T S_w w_i} \tag{20}$$

According to the nature of the ‘‘generalized Rayleigh quotient’’, the minimum value of J^* is the minimum eigenvalue of $S_w^{-1}S_b$. Afterwards, the unsupervised component of the loss function for CNN is obtained, as shown in Eq. (21).

$$\min(J^*) = \min[\text{eig}(S_w^{-1}S_b)] \quad (21)$$

Because of the simplicity and convergence rate of the cross-entropy function, we utilize it to construct the supervised component of the loss function for CNN, as shown in Eq. (22).

$$E_0 = -\frac{1}{N} \sum_x \sum_K y_k \ln a_k + (1 - y_k) \ln(1 - a_k) \quad (22)$$

Where (y_1, y_2, \dots, y_K) represents the expected output of CNN and (a_1, a_2, \dots, a_K) denotes the actual output. Based on Eqs. (21) and (22), the loss function of CNN is the sum of the two components:

$$E = [-\frac{1}{N} \sum_x \sum_K y_k \ln a_k + (1 - y_k) \ln(1 - a_k)] + \min[\text{eig}(S_w^{-1}S_b)] \quad (23)$$

After the training process has been achieved, the test samples are the input of the CNN model, and the predicted labels are obtained.

4. Experiments

The experiments consist of two parts. First, we discuss the effectiveness of the relevant steps in our method. Then we compare the performance of our method with that of the other semi-supervised methods. The experiments are performed on the Moving and Stationary Target Acquisition and Recognition (MSTAR) dataset which contains multiple types of targets. In our experiments, we choose ten types of targets, namely, 2S1, ZSU234, BRDM2, BTR60, BMP2, BTR70, D7, ZIL131, T62 and T72. Figure 3 shows the SAR and optical images of each type. Although the optical images are distinct from each other, the corresponding SAR images are difficult to be recognized because of the imaging nature. The dataset used in this paper consists of

the training and testing datasets. The detailed information is listed in Table 1.



Figure 3: The SAR and optical images of ten types of targets in the MSTAR dataset.

Table 1: The training and testing datasets of our experiment.

Type	Tops	Model	Training set		Testing set	
			Depression	Number	Depression	Number
2S1	Artillery	B_01	17°	299	15°	274
ZSU234		D_08	17°	299	15°	274
BRDM2		E_71	17°	298	15°	274
BTR60	Truck	K10YT_7532	17°	256	15°	195
BMP2		SN_9563	17°	233	15°	195
BTR70		C_71	17°	233	15°	196
D7	Tank	92V_13015	17°	299	15°	274
ZIL131		E_12	17°	299	15°	274
T62		A_51	17°	299	15°	273
T72	#A64	17°	232	15°	196	
Sum:2747					Sum:2425	

4.1 Evaluation of our method

4.1.1 Evaluation of the new LDA method

In our method, a new LDA method is designed to utilize the unlabelled samples. First, in order to verify the effectiveness of the proposed LDA method, we compare the overall accuracy

and the Kappa coefficients of our method with those of the supervised CNN method which only utilizes the labelled samples. The overall accuracy refers to the ratio of the number of correctly recognized samples to the number of all the samples. The calculation of Kappa coefficient is based on the confusion matrix, which can well represent the recognition accuracy of each class. The definition of Kappa coefficient is shown in Eq. (24), where p_o is the relative observed agreement between the recognition results for the test data and the real labels, and p_e represents the hypothetical probability of the chance agreement.

$$k = \frac{P_o - P_e}{1 - P_e} \quad (24)$$

In the experiments, the training dataset is divided into a labelled dataset L and an unlabelled dataset U . During the partition, we randomly select the same number of the samples from each class in the training dataset, and L consists of the selected samples. U consists of the remaining samples in the training dataset. We design six different partitions and the corresponding numbers of the samples in L and U are shown in Table 2. The Adam optimizer is adopted when we train the CNN, and the parameters are set experimentally as follows: $\eta = 0.001$, $\beta_1 = 0.9$, $\beta_2 = 0.99$. When performing the thresholding processing on the class probabilities, the value of t is set to 0.2. We repeated the experiments under different partitions for ten times and the average results are shown in Table 3.

Table 2: Six different partitions of the training dataset and the corresponding numbers of samples in L and U.

	Number of L	Number of U
1	300	2447
2	400	2347
3	500	2247
4	600	2147
5	800	1947
6	1000	1747

Table 3: The performance of the supervised CNN method and our method under different partitions of the training dataset. The supervised CNN method only utilizes the labelled samples while our method utilize both the labelled and unlabelled samples.

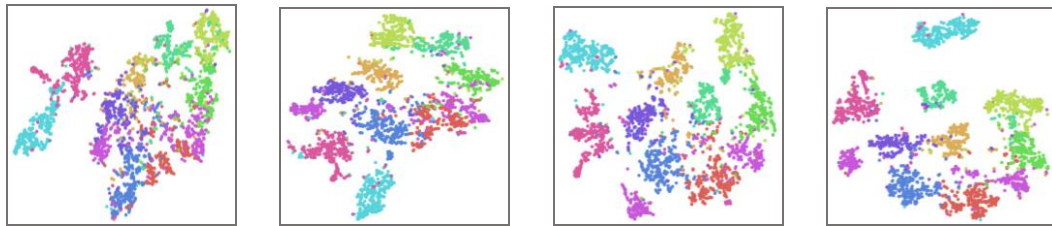
Training set	L:300, U:2447		L:400, U:2347		L:500, U:2247		L:600, U:2147		L:800, U:1947		L:1000, U:1747	
Method	CNN	Ours	CNN	Ours	CNN	Ours	CNN	Ours	CNN	Ours	CNN	Ours
2S1	0.70	0.73	0.68	0.79	0.77	0.84	0.83	0.87	0.84	0.89	0.91	0.95
BMP2	0.64	0.69	0.74	0.85	0.81	0.95	0.88	0.92	0.89	0.95	0.91	0.97
BRDM2	0.63	0.77	0.77	0.86	0.84	0.88	0.86	0.90	0.91	0.92	0.86	0.95
BTR70	0.58	0.74	0.76	0.89	0.79	0.89	0.81	0.90	0.89	0.94	0.88	0.96
BTR60	0.64	0.67	0.81	0.88	0.79	0.86	0.86	0.87	0.90	0.93	0.91	0.95
D7	0.88	0.89	0.91	0.92	0.96	0.97	0.96	0.96	0.97	0.98	0.99	0.98
T62	0.64	0.73	0.76	0.83	0.79	0.81	0.87	0.87	0.86	0.89	0.91	0.94
T72	0.55	0.64	0.70	0.82	0.80	0.87	0.83	0.87	0.84	0.92	0.89	0.94
ZIL131	0.59	0.71	0.75	0.87	0.77	0.86	0.74	0.86	0.83	0.90	0.88	0.92
ZSU234	0.75	0.81	0.86	0.90	0.91	0.90	0.91	0.93	0.94	0.96	0.96	0.97
Overall accuracy	0.67	0.74	0.78	0.86	0.83	0.88	0.85	0.90	0.89	0.93	0.91	0.95
Kappa score	0.63	0.71	0.75	0.85	0.81	0.87	0.84	0.88	0.87	0.92	0.90	0.95

As can be seen, the overall accuracy and the Kappa coefficients of our method outperforms those of the supervised CNN method. The fewer the labelled samples, the more significant the difference of the performance. And the difference gradually decreases as the number of the labelled samples increases. The reason is that, compared with the supervised CNN method, our method utilizes the unlabelled samples effectively. As a result, the generalization ability of our method is enhanced and the overall accuracy and the Kappa coefficients are improved. With the increasing labelled samples, the generalization ability of the CNN model is gradually augmented, hence the performance difference between the two methods decreases.

Next, we illustrate the effectiveness of the new LDA method. We extract the 1×10 feature vectors of the testing samples from the output of our method and the supervised CNN method. Then we transform the feature vectors to two-dimensional ones using the t-Distributed Stochastic Neighbor Embedding (t-SNE) method. In the experiment, we use the fourth partition of the

training dataset shown in Table 2 to train the two methods. The supervised CNN method only utilizes the labelled samples while our method utilize both the labelled and unlabelled samples. The distribution of the feature vectors from the output of our method and the supervised CNN method are shown in Figure 4. Different colors represent different classes. As can be seen, compared with the supervised CNN method, our method can effectively reduce the distance between the samples of the same class and increase the distance between the samples of different classes. Hence, the recognition accuracy of our method is improved, which is consistent with the experimental results shown in Table 3.

(I) CNN:



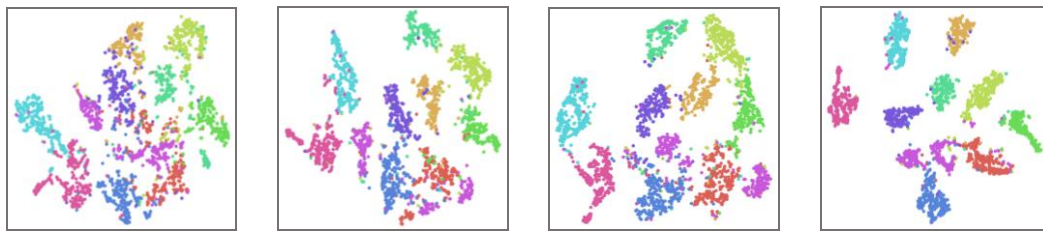
(1) L:400

(2) L:600

(3) L:800

(4) L:1000

(II) Ours:



(5) L:400, U:2347

(6) L:600, U:2147

(7) L:800, U:1947

(8) L:1000, U:1747

Figure 4: The distribution of the feature vectors from the output of our method and the supervised CNN method.

The first row represents the supervised CNN method's outcome and the second row represents our method's outcome. Different colors represent different classes.

4.1.2 Evaluation of the thresholding processing

After the class probabilities have been obtained, thresholding processing is applied to

improving the reliability of the unlabelled samples. Next, the effectiveness of the thresholding processing is discussed. We select two partitions of the training dataset shown in Table 2 to train our method, and the number of the samples in U is 2347 and 1947, respectively. In the experiment, we utilize the softmax function to calculate the class probabilities of the unlabelled samples. Then the reliability factors (RF) of the unlabelled samples are obtained based on the class probabilities and the true labels. We regard the samples with a RF value greater than 0.9 as reliable samples, and the remaining samples are regarded as unreliable samples. In the thresholding processing, we set the threshold t as 0, 0.2, 0.7 and 1, respectively. During the experiment, we record the number of the reliable samples, unreliable samples and available samples in U with different thresholds. The experimental results are shown in Table 4.

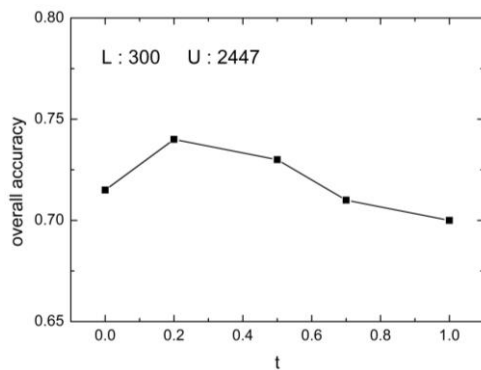
Table 4: The number of the reliable samples, unreliable samples and available samples in the unlabelled dataset with different thresholds.

Training set	L:400, U:2347				L:800, U:1947			
Threshold	t=0	t=0.2	t=0.7	t=1	t=0	t=0.2	t=0.7	t=1
Unreliable samples	329	259	198	20	125	112	80	8
Reliable samples	2018	2088	2034	891	1822	1835	1841	1646
Available samples	2347	2347	2232	911	1947	1947	1921	1654

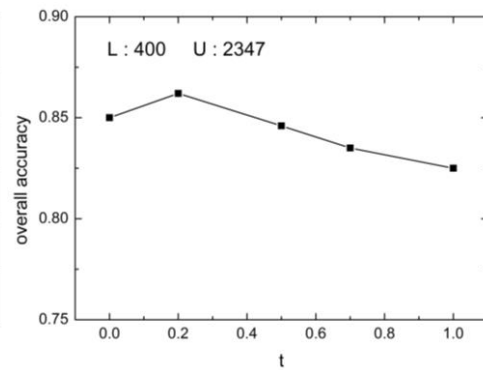
As can be seen, if the threshold is set to 0, there will be more unreliable samples. As the threshold increases, the reliability of the unlabelled samples is improved. Compared with the case of $t=0$, when $t=0.2$, the number of the unreliable samples is reduced, and the number of the reliable samples is increased. Hence, the thresholding processing can effectively improve the reliability of the unlabelled samples. However, if the threshold continues to increase, the number of the available samples is gradually reduced. The reason is that, if the maximum probability of a sample is less than the threshold, all the probabilities of the sample are set to 0. As shown in

Figure 1, we utilize the unlabelled samples based on the class probabilities and the new LDA method. The unlabelled samples, whose class probabilities are all set to 0, will not be utilized in the training process. Therefore, as the threshold increases, the number of the available unlabelled samples drops.

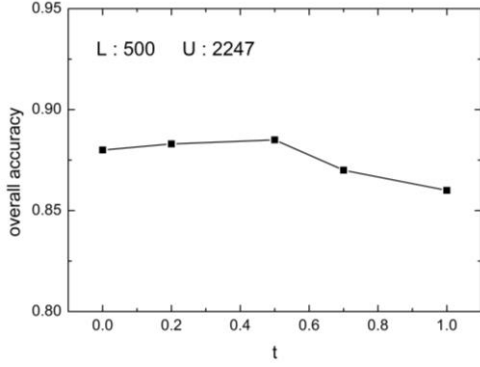
Next, we analyze the performance of our method with different thresholds. The experimental results are shown in Figure 5. When the number of the labelled samples is less than 500, the performance of our method is better whilst the threshold is set to be 0.2. As the number of the labelled samples increases, the recognition accuracy is almost the same at different thresholds, in other words, the impact of the thresholding processing becomes weak. This is because the generalization ability of the CNN model is weak when the labelled samples are insufficient. Compared with the case of $t=0$, setting $t=0.2$ helps to improve the reliability of the unlabelled samples. Thus, the recognition accuracy is improved. However, if we continue to increase the threshold, the number of the available unlabelled samples drops and the recognition accuracy become worse. As the number of the labelled samples increases, the generalization ability of the CNN model is improved. As a result, the reliability of the unlabelled samples is improved, and the impact of thresholding processing is weaker. Thus, in order to achieve the best recognition performance, the threshold should be set to 0.2.



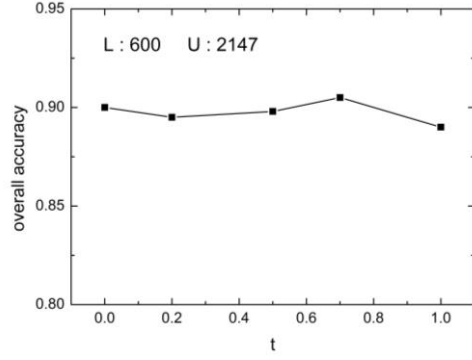
(1)



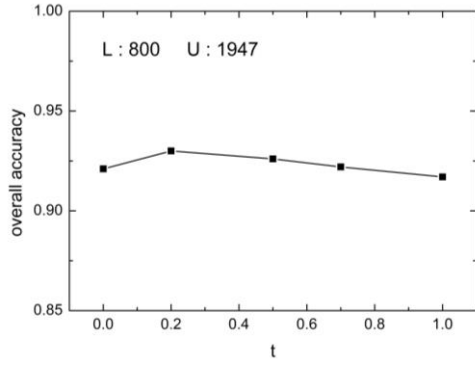
(2)



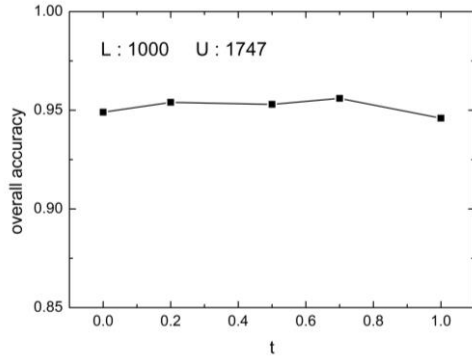
(3)



(4)



(5)



(6)

Figure 5: The recognition accuracy of our method at different thresholds and different training dataset partitions.

4.2 Comparison with other semi-supervised methods

In this section, we compare the performance of our method with that of the semi-supervised ladder network model [25], Pi model and temporal ensembling model [26]. The semi-supervised ladder network model combines the semi-supervised learning and deep learning methods. Based on the self-ensembling method, the Pi and temporal ensembling models are both semi-supervised CNN methods.

4.2.1 Recognition accuracy

First, we compare the overall accuracy of these methods. As shown in Figure 6, our method outperforms the semi-supervised ladder network. The reason is that the ladder network is composed of fully connected layers whose feature extraction ability is weaker than that of the

CNN model used in our method. Furthermore, our method is superior to the other two models. This because the Pi and temporal ensembling models utilize the CNN to predict the labels of the unlabelled samples. According to the predicted labels, the unlabelled component of the loss function is obtained. However, if the initial labelled samples are insufficient, the generalization ability of the CNN is weak. Therefore, the reliability of the predicted labels is low and the unlabelled samples are not contributing to the augmentation of the system performance. In contrast, our method can accurately estimate the class probabilities of the unlabelled samples. Based on the class probabilities, the impact of the unlabelled samples is well controlled in the training process. As a result, the reliability of the unlabelled samples is improved and the recognition accuracy is increased.

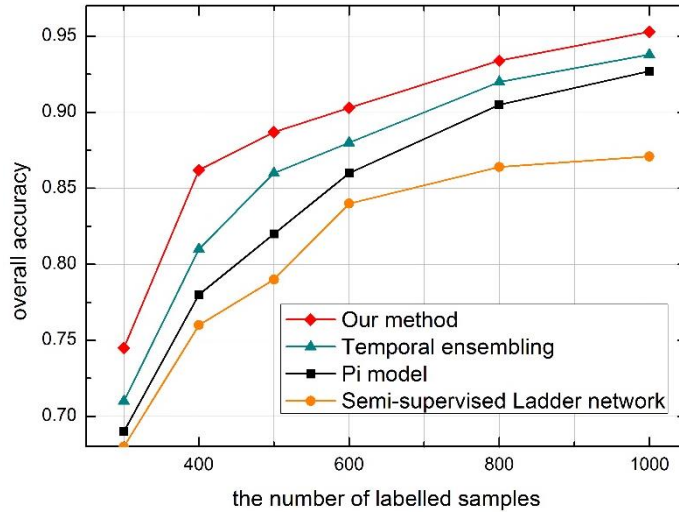


Figure 6: The recognition accuracy of our method, temporal method, Pi model and semi-supervised ladder network with different partitions of the training dataset.

4.2.2 Training time

To evaluate the computation complexity of our method and the other three semi-supervised methods, we calculate the average training time for each epoch. During the training process, the numbers of samples in L and U are 600 and 2147, respectively. The number of the epochs is

set to 400. The experiments are implemented in the Pytorch 0.3.1 framework. And the main configurations of the computer are: GPU: Tesla K20c; video memory: 4G; operating system: Ubuntu 16.04.

Table 5: The running time of each epoch of our method, temporal method, Pi model and semi-supervised ladder network trained. All the four methods are trained by 600 labelled samples and 2147 unlabelled samples.

Methods	Training time (sec/epoch)
Our method	2.53
Temporal ensembling	1.56
Pi model	2.45
semi-supervised ladder network	5.08

As shown in Table 5, the average training time of our method is 2.53sec/epoch, much less than that of the semi-supervised ladder network. The reason is that the structure of the ladder network is complex than that of the CNN used in our method. Thus there are more parameters that need to be trained in the ladder network, resulting in longer training time. Besides, the average training time of the Pi model and temporal ensembling model is less than that of our method. This is because the Pi and temporal ensembling models utilize the CNN to predict the labels of the unlabelled samples. Afterwards, the unlabelled component of the loss function is obtained based on the predicted labels. Thus, the computation complexity of the two methods is less than our method. However, our method can effectively maintain the reliability of the unlabelled samples. Although the computation complexity of our method is increased, the recognition accuracy is also improved.

5. Conclusion

To effectively utilize the unlabelled samples, inspired by the neural network structure and the semi-supervised learning mechanism of the human cognitive system, a new semi-supervised CNN

method has been presented in this paper. In the training process, the class probabilities are utilized to control the impact of the unlabelled samples. As a result, the reliability of the unlabelled samples is enhanced and the SAR-ATR accuracy of our method is improved. The contributions of this paper are summarized as follows.

(1) We utilized the CNN to extract the features of the samples, and then the class probabilities of unlabelled samples were obtained by the softmax function.

(2) To improve the reliability of unlabelled samples, we performed thresholding processing on the class probabilities.

(3) Based on the class probabilities, a new LDA method was designed to utilize the unlabelled samples. As a result, the recognition accuracy was improved.

We performed the experiments on the MSTAR dataset. First, we verified the effectiveness of the relevant steps used in our method. Then we compared the performance of our method with that of the other semi-supervised methods. From the experimental results, we conclude that our method can effectively improve the SAR-ATR accuracy despite the lack of the labelled samples.

Acknowledgements

This research was funded by the National Natural Science Foundation of China (No.61771027, No.61071139, No.61471019, No.61501011, and No.61171122). E.

Yang is supported in part under the RSE-NNSFC Joint Project (2017-2019) (No.6161101383) with China University of Petroleum (Huadong).

H. Zhou was supported by UK EPSRC under Grant EP/N011074/1, Royal Society-Newton Advanced Fellowship under Grant NA160342, and European Union's Horizon 2020 research and innovation program under the Marie-Sklodowska-Curie grant agreement No 720325.

Compliance with Ethical Standards

Conflict of Interest

The authors declare that they have no conflict of interest.

Ethical Approval

This article does not contain any studies with human participants performed by any of the authors.

References

1. Moreira A, Prats-Iraola P, Younis M, Krieger G. A tutorial on synthetic aperture radar. *IEEE Geosci Remote Sens Mag* 2013;1(1):6-43.
2. Wang G, Tan S, Guan C, Wang N, Liu Z. Multiple model particle filter track-before-detect for range ambiguous radar. *Chin J Aeronaut* 2013;26:1477-87.
3. Gong M, Su L, Jia M, Chen W. Fuzzy clustering with a modified MRF energy function for change detection in synthetic aperture radar images. *IEEE Trans Fuzzy Syst* 2014;22:98-109.
4. Chen H, Zhang F, Tang B, Yin Q, Sun X. Slim and efficient neural network design for resource-constrained SAR target recognition. *Remote Sens* 2018;10(10):1-15.
5. Zhang F, Hu C, Yin Q, Li W, Li H, Hong W. Multi-aspect-aware bidirectional LSTM networks for synthetic aperture radar target recognition. *IEEE Access* 2017;5:26880-91.
6. Zhang S, He B, Rui N, Wang J, Han B, Lendasse A. Fast image recognition based on independent component analysis and extreme learning machine. *Cogn Comput* 2014;6(3):405-22.
7. Garagnani M, Wennekers T, Pulvermüller F. Recruitment and consolidation of cell assemblies for words by way of hebbian learning and competition in a multi-layer neural network. *Cogn Comput* 2009;1(2):160-76.
8. Yan X. Dissociated emergent-response system and fine-processing system in human neural network and a heuristic neural architecture for autonomous humanoid robots. *Comput Intell Neurosci* 2011;3(2):367-73.
9. Gao F, Ma F, Zhang Y, Wang J, Sun J, Yang E, Hussain A. Biologically inspired progressive enhancement target detection from heavy cluttered sar images. *Cogn Comput* 2016;8(5):955-66.

10. Spratling M. A hierarchical predictive coding model of object recognition in natural images. *Cogn Comput* 2017;9(2):151-67.
11. Ren P, Sun W, Luo C, Hussain A. Clustering-oriented multiple convolutional neural networks for single image super-resolution. *Cogn Comput* 2018;10(1):165-78.
12. Chen Y, Jiang H, Li C, Jia X, Ghamisi P. Deep feature extraction and classification of hyperspectral images based on convolutional neural networks. *IEEE Trans on Geosci Remote Sensing* 2016;54(10):6232-51.
13. Amrani M, Jiang F. Deep feature extraction and combination for synthetic aperture radar target classification. *J Appl Remote Sens* 2017;11(4):1.
14. Zhao J, Guo W, Cui S, Zhang Z, Yu W. Convolutional neural network for SAR image classification at patch level. *Geoscience and Remote Sensing Symposium IEEE* 2016;945-8.
15. Chen S, Wang H. SAR target recognition based on deep learning. *International Conference on Data Science and Advanced Analytics IEEE* 2015;541-7.
16. Gao F, Huang T, Sun J, Wang J, Hussain A, Yang E. A new algorithm of SAR image target recognition based on improved deep convolutional neural network. *Cogn Comput* 2018;1-16.
17. Liu B, Yu X, Zhang P, Tan X, Yu A, Xue Z. A semi-supervised convolutional neural network for hyperspectral image classification. *Remote Sens Lett* 2017;8(9):839-48.
18. Fu Z, Zhang F, Yin Q, Li R, Hu W, Li W. Small sample learning optimization for resnet based sar target recognition. *International Geoscience and Remote Sensing Symposium IEEE* 2018;2330-3.
19. Zhu X, Rogers T, Qian R, Kalish C. Humans perform semi-supervised classification too. *National Conference on Artificial Intelligence AAAI Press* 2007;864-9.

20. Haeusser P, Mordvintsev A, Cremers D. Learning by association — a versatile semi-supervised training method for neural networks. In Proceedings of IEEE conference on computer vision and pattern recognition 2017;626-35.
21. Gibson B, Rogers T, Zhu X. Human semi-supervised learning. Top Cogn Sci 2013;5(1):132-72.
22. Hänsch R, Hellwich O. Semi-supervised learning for classification of polarimetric SAR-data. Geoscience and Remote Sensing Symposium IEEE 2010;987-90.
23. Uhlmann S, Kiranyaz S, Gabbouj M. Semi-supervised learning for ill-posed polarimetric SAR classification. Remote Sens 2014;6(6):4801-30.
24. Basu S. Semi-supervised learning. Pacific-Asia Conference on Advances in Knowledge Discovery and Data Mining 2010;588-95.
25. Leng Y, Xu X, Qi G. Combining active learning and semi-supervised learning to construct SVM classifier. Knowledge-Based Syst 2013;44:121-31.
26. Zhang X, Song Q, Liu R, Wang W, Jiao L. Modified co-training with spectral and spatial views for semisupervised hyperspectral image classification. IEEE J. Sel. Top. Appl. Earth Observ. Remote Sens 2014; 7(6):2044-55.
27. Lv L, Zhao D, Deng Q. A semi-supervised predictive sparse decomposition based on task-driven dictionary learning. Cogn Comput 2016;9(1):1-10.
28. Ding S, Xi X, Liu Z, Qiao H, Zhang B. A novel manifold regularized online semi-supervised learning model. Cogn Comput 2018;10(1):49-61.
29. Rasmus A, Valpola H, Honkala M, Berglund M, Raiko T. Semi-supervised learning with ladder networks. Compu Sci 2015;9 Suppl 1(1):1-9.

30. Laine S, Aila T. Temporal ensembling for semi-supervised learning. International Conference on Learning Representations 2017.
31. Le T, Kim S. A hybrid selection method of helpful unlabeled data applicable for semi-supervised learning algorithms. The IEEE International Symposium on Consumer Electronics 2014;1-2.
32. Li Y, Zhou Z. Towards making unlabeled data never hurt. IEEE Trans Pattern Anal Mach Intell 2015; 37(1):175–88.
33. Szegedy C, Liu W, Jia Y, Sermanet P, Reed S, Anguelov D. Going deeper with convolutions. IEEE Conference on Computer Vision and Pattern Recognition 2015;1-9.
34. Lawrence S, Giles C, Tsoi C, Back A. Face recognition: a convolutional neural-network approach. IEEE Trans on Neural Netw 1997;8(1):98-113.
35. Moskowitz L. The LDA - an integrated diagnostics tool. IEEE Aerosp Electron Syst Mag 1986;1(7):22-6.
36. Huan R, Liang R, Pan Y. SAR target recognition with the fusion of LDA and ICA. International Conference on Information Engineering and Computer Science IEEE 2009;1-5.